

## Direct measurement of thin-film thermoelectric figure of merit

Rajeev Singh,<sup>1,a)</sup> Zhixi Bian,<sup>1</sup> Ali Shakouri,<sup>1</sup> Gehong Zeng,<sup>2</sup> Je-Hyeong Bahk,<sup>2</sup> John E. Bowers,<sup>2</sup> Joshua M. O. Zide,<sup>3</sup> and Arthur C. Gossard<sup>3</sup>

<sup>1</sup>*Baskin School of Engineering, University of California, Santa Cruz, California 95064, USA*

<sup>2</sup>*Department of Electrical and Computer Engineering, University of California, Santa Barbara, California 93106, USA*

<sup>3</sup>*Department Materials, University of Santa Barbara, California 93106, USA*

(Received 20 October 2008; accepted 13 February 2009; published online 28 May 2009)

We utilize the transient Harman technique to measure the thermoelectric figure of merit of thin films. A device structure is designed and fabricated to extract the thermoelectric properties of 20  $\mu\text{m}$  thick film composed of InGaAlAs semiconductor with embedded ErAs nanoparticles. High-speed voltage measurements with 63 dB of dynamic range and 200 ns resolution are achieved. Surface temperature measurements of the devices are used to extract the cross-plane Seebeck coefficient and thermal conductivity of the thermoelectric material. Self-consistent finite-element simulations of the three-dimensional temperature distributions in the active devices are in close agreement with the experimental thermal maps. © 2009 American Institute of Physics. [DOI: 10.1063/1.3094880]

Thermoelectric materials are playing an increasingly important role in a technologically advanced and resource-limited world. An important application of thermoelectric materials is in direct thermal-to-electrical energy conversion. Because a substantial amount of energy in our world is in thermal form, there are tremendous applications for thermoelectric devices that efficiently convert thermal energy into electricity. The energy conversion efficiency of a thermoelectric material is a function of its dimensionless figure of merit that is defined as  $ZT \equiv S^2 \sigma T / \kappa$ , where  $S$ ,  $\sigma$ ,  $\kappa$ , and  $T$  are the material's Seebeck coefficient, electrical conductivity, thermal conductivity, and ambient temperature, respectively. The numerator of  $ZT$  is known as the thermoelectric power factor ( $P$ ). Recent work to improve the  $ZT$  of materials designed for high-temperature power generation has focused on thin films due to the freedom to engineer the materials at the nanoscale. In bulk thermoelectric materials, there is a dramatic tradeoff between  $S$  and free carrier concentration ( $n$ ). Therefore,  $n$  is chosen to optimize  $P$  at a particular  $T$ . Efforts have been made to decouple  $S$  and  $n$  to increase the  $P$  of thin films beyond bulk values using low dimensional structures or with electronic energy filtering for large  $n$  in tall barrier heterostructures.<sup>1</sup> However, the majority of improvement in  $ZT$  has been achieved through the reduction in  $\kappa$  due to interfacial phonon scattering. An extension of this concept was recently demonstrated in isotropic nanoparticle thin films that exhibit a  $\kappa$  that is a factor of 2 below the bulk alloy limit due to enhanced scattering of longer wavelength phonons.<sup>2</sup> This reduction in  $\kappa$  is achieved while enhancing  $\sigma$  due to an increase in  $n$  by the semimetallic nanoparticles. Nanostructured thin-film research offers great potential to increase the  $ZT$  of thermoelectric materials.

Accurate characterization of thin film thermoelectrics is an important step in the development of these materials. In order to evaluate the  $ZT$  of thin films, we utilize direct cross-plane  $ZT$  measurement using the Harman method.<sup>3</sup> The Harman method utilizes measurements of transient voltages in a thermoelectric device to extract the resistive voltage drop

and the Seebeck-induced voltage drop (slower thermal response). Further study of the Seebeck voltage under opposite polarities permits the separation of the Joule effect-induced and the Peltier effect-induced Seebeck voltages. However, the Harman method is quite difficult to apply to thin films. Due to the fast thermal response of thin films, high-speed detection of the small transient Seebeck voltage is necessary.<sup>4</sup> In addition, because this method relies on closed-circuit electrical measurements, electrical parasitics such as resistances in series with the material under investigation will result in a reduction in the measured  $ZT$  relative to the intrinsic material value. Additionally, the side of the measurement device that is not heat-sinked must be free of any parasitic heat load, making electrical probing difficult for the requirement of uniform device current injection.

Specific device geometries are used to obtain accurate measurement of the cross-plane  $ZT$  of InGaAlAs thin films with embedded ErAs nanoparticles (Fig. 1). The devices are

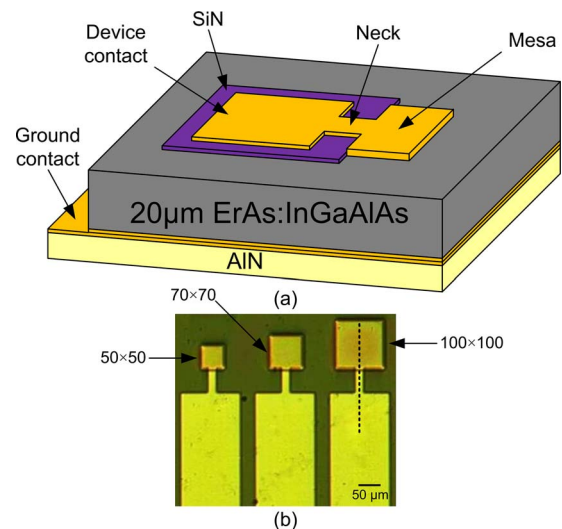


FIG. 1. (Color online) (a) Diagram of device designed for direct measurement of the cross-plane  $ZT$  of ErAs:InGaAlAs thin-film thermoelectric material. (b) Magnified optical image of patterned devices of different mesa areas.

<sup>a)</sup>Electronic mail: rsingh@soe.ucsc.edu.

fabricated to minimize electrical parasitics through removal of the growth substrate. In addition, it is important to optimize the geometry of the electrical lead used to apply current to the top contact area. The parasitic heat conduction from the device mesa through the metal lead should be minimized while maintaining current injection uniformity throughout the device area. In-plane measurement of electrical conductivity using the open-circuit van der Pauw<sup>5</sup> technique is compared to the value obtained in the cross-plane direction using the transient method in order to characterize the electrical parasitics in series with devices. Thermal imaging of the device is accomplished to determine the temperature distribution on the mesa and along the metal lead due to the Peltier and Joule effects. Independent measurements of the material's in-plane Seebeck coefficient and electrical conductivity are used in self-consistent finite-element method (FEM) simulations to calculate the measured thermal profile on the metallization of devices of different areas.

N-type  $(\text{In}_{0.53}\text{Ga}_{0.38}\text{Al}_{0.09}\text{As})_{0.997}\text{ErAs}_{0.003}$  film 20  $\mu\text{m}$  thick is grown lattice-matched to (100) InP semi-insulating substrate between 250 nm thick highly doped InGaAs buffer and cap layers using molecular beam epitaxy.<sup>6-8</sup> The buffer and cap layers serve as electrical contact layers. In-plane measurement samples have the same active film composition without the buffer and cap layers. Devices with van der Pauw geometry are fabricated by depositing Ti/Au electrical contacts using an electron beam evaporator. The sample is subsequently passivated with a 300 nm thick layer of  $\text{Si}_3\text{N}_4$ . Cross-plane  $ZT$  measurement devices are fabricated by depositing a uniform Ti/Au layer 3  $\mu\text{m}$  thick on the cap layer. The wafer is then flip-chip bonded to a Au-coated AlN chip carrier. The 520  $\mu\text{m}$  thick InP substrate is then etched away using a HCl solution to reveal the highly doped buffer layer. Finally, Ti/Au contacts are deposited and patterned using standard photolithographic techniques with  $\text{Si}_3\text{N}_4$  serving to insulate the metal contact leads from the film. The contact resistivity measured using transmission line patterns is in the order of  $10^{-7} \Omega \text{ cm}^2$ .<sup>9</sup> Figure 1(a) is a diagram of a device and Fig. 1(b) is a magnified optical image of patterned devices of different mesa areas.

In order for the transient Harman method to be valid experimentally, heat transfer between the hot and cold sides of the thermoelectric device must only occur through the thin film, i.e., thermal shunting of the film must not occur. In addition, current injection uniformity through the top metal contact must be achieved. However, when the device's aspect ratio decreases, current injection uniformity can decrease with thermal leakage via the metal lead. Due to the coupling of thermal leakage and current uniformity, metal lead geometry and thickness are optimized in an attempt to achieve both conditions. The optimized metal lead geometry that serves to thermally isolate the device mesa from its contact pad is shown in Fig. 1(b). Current injection variation through a  $100 \times 100 \mu\text{m}^2$  device mesa is measured as less than 6% by scanning a probe on the mesa while detecting the transient resistive voltage component due to an electric current pulse at each location.

The cross-plane Seebeck coefficient of the film is calculated from a measured transient Seebeck voltage of  $-420 \mu\text{V}$  and a  $\Delta T$  of 1.8 K (measured using a microthermocouple) for a  $100 \times 100 \mu\text{m}^2$  area device at a current of 100 mA at 300 K. The resulting Seebeck of  $-233 \mu\text{V K}^{-1}$

agrees well with the measured in-plane value of  $-224 \mu\text{V K}^{-1}$ , indicating that ErAs:InGaAlAs has an isotropic Seebeck coefficient. The in-plane electrical conductivity is measured to be  $348 \Omega^{-1} \text{ cm}^{-1}$  at 300 K using the van der Pauw method. Due to three-dimensional (3D) electric current and heat flux spreading in the film, the effective device area is greater than the cross section defined by the mesa area. A spreading factor  $C$  is introduced in the equation for device resistance, given as

$$R = C \frac{1}{\sigma A} d + R_s, \quad (1)$$

where  $R$  is the electrical or thermal resistance of the film whose cross section is defined by the mesa area  $A$ ,  $\sigma$  is the electrical conductivity of the material,  $d$  is the film thickness, and  $R_s$  is the parasitic series resistance. The spreading factor  $C$  is calculated using the FEM as 0.79 for a mesa area of  $100 \times 100 \mu\text{m}^2$  and a film thickness of 20  $\mu\text{m}$ . The electrical resistance of the  $100 \times 100 \mu\text{m}^2$  device is measured to be 69 m $\Omega$  at 300 K by transient measurement directly on the mesa in order to eliminate the contribution of the lead resistance.  $R_s$  is estimated by measuring the resistance of three device areas ( $50 \times 50$ ,  $70 \times 70$ , and  $100 \times 100 \mu\text{m}^2$ ) and fitting these measurements with Eq. (1). A parasitic series resistance of 23 m $\Omega$  is determined. The cross-plane electrical conductivity is then calculated to be  $347 \Omega^{-1} \text{ cm}^{-1}$ . Equation (1) neglects the insignificant contact resistivity. The cross-plane conductivity is in good agreement with the in-plane value of  $348 \Omega^{-1} \text{ cm}^{-1}$  measured using the van der Pauw method.

The FEM simulations of the thermoelectric devices utilize coupled heat and electric field equations given as

$$C_h \frac{\partial T}{\partial t} = \nabla(\kappa \nabla T) + J^2 \sigma^{-1} - JT \nabla S \quad (2)$$

and

$$F = J\sigma^{-1} + S \nabla T, \quad (3)$$

where  $C_h$ ,  $\kappa$ ,  $\sigma$ , and  $S$  are the specific heat capacity, thermal conductivity, electrical conductivity, and Seebeck coefficient, respectively, of the material,  $T$  is the local temperature,  $J$  is the electric current density, and  $F$  is the electric field. The first, second, and third terms on the right-hand side of Eq. (2) account for the heat fluxes in the thermoelectric device that are due to thermal conduction, Joule heating, and Peltier heating/cooling, respectively.<sup>10</sup> The first and second terms on the right-hand side of Eq. (3) account for the components of the electric field in the thermoelectric device that are due to electrical resistance and the Seebeck effect, respectively. The coupled equations are solved iteratively until convergence to steady-state temperature and voltage distributions. The full 3D FEM calculations consider parasitic heat conduction via the metal lead as well as heat conduction in the film and  $\text{Si}_3\text{N}_4$  layer, distributed Joule heating, Peltier cooling/heating, as well as the effect of induced Seebeck voltages on the electric flux. Figure 2 is the measured and calculated thermal profiles for different device areas along the long axis of the devices from the contact pad to the mesa as indicated by the dashed line in Fig. 1(b). The thermal profiles are measured using thermoreflectance and the Peltier and Joule components are separated by lock-in detection, respectively, of the first and second harmonics of the thermal signal induced

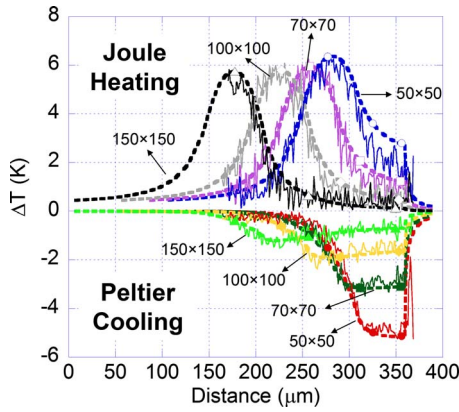


FIG. 2. (Color online) Measured (solid lines) and calculated (dashed lines) thermal profiles along the long axis of devices of different areas for a sinusoidal current amplitude of 100 mA.

by a bipolar and symmetric sinusoidal current amplitude of 100 mA at 100 Hz. The simulated thermal profiles are in excellent agreement with the measured values provided that the material property values listed in Table I as “FEA calculation parameters” are used in the calculation. The values used in the calculation are in good agreement with the measured in-plane Seebeck coefficient and electrical conductivity values. However, the room-temperature cross-plane thermal conductivity of  $5.0 \text{ W m}^{-1} \text{ K}^{-1}$  is substantially larger than the value of  $3.0 \text{ W m}^{-1} \text{ K}^{-1}$  measured using the  $3\omega$  technique on a  $1.6 \mu\text{m}$  thick film.<sup>2</sup> Using the measured in-plane Seebeck coefficient value of  $-224 \mu\text{V K}^{-1}$  and the measured cross-plane  $\Delta T$  of 1.8 K, the cross-plane thermal conductivity is calculated using the cooling power equation of an ideally heat-sinked thermoelectric device under zero heat load<sup>10</sup> as

TABLE I. Summary of measured ErAs:InGaAlAs material parameters extracted from in-plane and cross-plane measurements at 300 K as well as the values used in the FEM simulation of the thermal profiles on the device metallization.

Data source	Seebeck coefficient ( $\mu\text{V K}^{-1}$ )	Electrical conductivity ( $\Omega^{-1} \text{ cm}^{-1}$ )	Thermal conductivity ( $\text{W m}^{-1} \text{ K}^{-1}$ )
In-plane measurement data	-224	348	N/A
Cross-plane measurement data	-233	258	5.9
FEA calculation parameter	-220	330	5

$$\kappa = C \frac{1}{\Delta T} |STI| \frac{d}{A}, \quad (4)$$

(the variables are as previously defined) resulting in a thermal conductivity of  $5.9 \text{ W m}^{-1} \text{ K}^{-1}$  for the  $100 \times 100 \mu\text{m}^2$  area device. Because Eq. (4) does not consider the effect of heat conduction through the device’s metal lead, the actual material thermal conductivity will be less. In comparison, the calculated thermal conductivities for the  $50 \times 50$  and  $70 \times 70 \mu\text{m}^2$  area devices are 6.8 and  $6.1 \text{ W m}^{-1} \text{ K}^{-1}$ , respectively. Finite-element simulation estimates the thermal leakage via the metal lead at the operating current to be 29.91%, 19.58%, and 16.55% of the total Peltier effect-induced heat flux for the  $50 \times 50$ ,  $70 \times 70$ , and  $100 \times 100 \mu\text{m}^2$  area devices, respectively. The increase in thermal conductivity relative to the reported value of  $3 \text{ W m}^{-1} \text{ K}^{-1}$  measured using the  $3\omega$  technique may be due to the affect of growth characteristics of the much thicker  $20 \mu\text{m}$  film.<sup>9</sup> Recent measurements have shown that thin digitally grown layers indeed have lower thermal conductivities than thicker films grown by analog depositions. This is due to the contribution of phonons with long mean free paths and also due to the additional scattering at the digital growth superlattice interfaces.

This work was supported by ONR MURI Thermionic Energy Conversion Center.

- <sup>1</sup>D. Vashaee and A. Shakouri, *Phys. Rev. Lett.* **92**, 106103 (2004).
- <sup>2</sup>W. Kim, J. Zide, A. Gossard, D. Klenov, S. Stemmer, A. Shakouri, and A. Majumdar, *Phys. Rev. Lett.* **96**, 045901 (2006).
- <sup>3</sup>T. C. Harman, *J. Appl. Phys.* **29**, 1373 (1958).
- <sup>4</sup>R. Singh, Z. Bian, G. Zeng, J. Zide, J. Christofferson, H.-F. Chou, A. Gossard, J. Bowers, and A. Shakouri, Proceedings of MRS Fall Meeting, Boston, November 2005 (unpublished).
- <sup>5</sup>L. J. van der Pauw, *Philips Res. Rep.* **13**, 1 (1958).
- <sup>6</sup>D. C. Driscoll, M. Hanson, C. Kadow, and A. C. Gossard, *Appl. Phys. Lett.* **78**, 1703 (2001).
- <sup>7</sup>D. C. Driscoll, M. P. Hanson, E. Mueller, and A. C. Gossard, *J. Cryst. Growth* **251**, 243 (2003).
- <sup>8</sup>J. M. Zide, D. O. Klenov, S. Stemmer, A. C. Gossard, G. Zeng, J. E. Bowers, D. Vashaee, and A. Shakouri, *Appl. Phys. Lett.* **87**, 112102 (2005).
- <sup>9</sup>G. Zeng, J.-H. Bahk, J. M. O. Zide, Z. Bian, R. Singh, W. Kim, S. L. Singer, A. Majumdar, A. Shakouri, A. C. Gossard, and J. E. Bowers, *Appl. Phys. Lett.* **91**, 263510 (2007).
- <sup>10</sup>G. S. Nolas, J. Sharp, and J. Goldsmid, *Thermoelectrics: Basic Principles and New Materials Developments* (Springer, Berlin, 2001).